COMPUTATIONAL STUDY OF CHEMICALLY REACTING HYPERSONIC FLOW

Yoshifuru Funahashi
Department of Aeronautics and Astronautics, Graduate School of Engineering,
The University of Tokyo, Tokyo, JAPAN

Keywords: *Hypersonic flow, Chemical equilibrium, Thermal protection*

Abstract

Because space vehicles reentering the Earth's atmosphere are exposed to immense aerodynamic heating, so some kinds of thermal protection systems are indispensable. Computational analysis of two kinds of thermal protection systems, that is, the film cooling and the transpiration cooling, was conducted, taking real gas effects into account.

1 General Introduction

1.1 Thermal Protection Systems

Because space vehicles reentering the Earth's atmosphere are exposed to immense aerodynamic heating, so some kinds of thermal protection systems are indispensable.

Currently, various types of thermal protection have been contrived. Among them, the ones that involve mass transfer are listed below:

- Film cooling
- Transpiration cooling
- Ablation cooling

Film cooling is a method of injecting coolant gas through some slits and making a thin film on the surface. The first injection point is usually set to the stagnation point, where the aerodynamic heating is the most severe. And in many cases, the second injection point is set to the point where the influence of the first injection becomes weak.

Transpiration cooling is a method to transpire a coolant air through a porous media in a wide area. Like as film cooling, the coolant air forms a thin film on the surface and makes the boundary layer thicker. The coolant air exchanges the heat with a material also in the matrix. Film cooling and transpiration cooling have the advantage of reusability and safety, but the systems are so complicated and hence costly.

Ablation cooling is a method that makes use of the sublimation of the resin called ablator. This method can save cost and weight and has high reliability, but the disadvantage is that the system cannot be reused.

1.2 Real Gas Effects

The gas temperature in the nose region of the vehicles is extremely high, so real gas effects such as chemical reactions occur. Under the

constant pressure of 1 atm, the vibrational energy of the molecules becomes significant at about 800K. When the temperature reaches about 2000 K, O_2 begins to dissociate. At 4000 K, N_2 begins to dissociate. At 9000 K, the oxygen and nitrogen ionization occurs. These phenomena make a great impact on the properties of the gas, and hence, on the flow. Therefore, the proper inclusion of real gas effects is vital to the calculation of the flow around the hypersonic vehicles.

1.3 Classification of the Flows

Chemically reacting flows can be classified into three types depending on the two characteristic times, that is, the characteristic time of the flow and the one of the chemical reaction. The characteristic time of the flow can be defined as the time it takes for a fluid element to traverse the flow field of interest. And the characteristic time of the chemical reaction can be defined as the time it takes for the chemical reactions to reach equilibrium. So, we can assume:

$\tau_f \ll \tau_c$: Frozen Flow

$\tau_f \approx \tau_c$: Nonequilibrium Flow

$\tau_f \gg \tau_c$: Equilibrium Flow

In this study, the present author analyzed the flow under the condition in which the assumption of the chemical equilibrium is valid.

1.4 Aerodynamic Heating

Aerodynamic heating consists of three kinds of heating, that is, conductive heating, diffusive heating, and radiative heating:

$$q = q_C + q_D + q_R \tag{1}$$

$$q_C = -\kappa \frac{\partial T}{\partial n} \tag{2}$$

$$q_D = \sum_i^N \rho_i \, d_i \, h_i \tag{3}$$

$$q_R = \int_0^{\infty} \int_0^{2\pi} \int_0^{\pi} I_\nu(\theta, \phi) \cos\theta \sin\theta \, d\theta \, d\phi \, d\nu \tag{4}$$

Conductive heating is caused by the temperature gradient and governed by Fourier's law.

For a chemically reacting mixture, there is also an energy transport due to diffusion. As species diffuse through the gas, the enthalpy of the species is carried with them. The heating caused by this phenomenon is called diffusive heating.

Moreover, when the temperature of the gas is extremely high, radiation becomes significant. For air, this threshold temperature is about 10,000 K. The radiation interacts with the flow field and creates the immense heating for the space vehicles. For example, for the Apollo reentry, the radiative heating was more than 30 percent of the total heating. But under the condition of this study, where the assumption of the chemical equilibrium holds, radiative heating can be neglected compared to conductive heating and diffusive heating.

2 Computational Method

2.1 Governing Equations

The governing equations for the external flow are the two dimensional axisymmetric Navier-Stokes equations:

$$\frac{\partial Q}{\partial t} + \frac{\partial E}{\partial x} + \frac{\partial F}{\partial y} + H = \frac{\partial E_v}{\partial x} + \frac{\partial F_v}{\partial y} + H_v \tag{5}$$

For the analysis of transpiration cooling, we must solve the internal flow and heat conduction of the porous media simultaneously with the external flow. Like as Navier-Stokes equations, the equations for the internal flow in the porous media also consist of the equation for mass conservation, the equations for motion and the equation for energy conservation. To model the flow in the porous media, we must define the porosity, ϕ, as the volume of the pore in the unit volume of the porous media. Then, the equation for mass conservation is:

$$\phi \frac{\partial \rho_f}{\partial t} + \nabla \bullet \left(\rho_f \mathrm{V}_f \right) = 0 \qquad (6)$$

The equation for motion is:

$$-\nabla p_f = \left(\alpha \mu_f + \beta \rho_f \left| \mathbf{V}_f \right| \right) \mathbf{V}_f \qquad (7)$$

The above equation is the empirical law called Darcy's law. α, β is the constant. [1] And the equation for the energy conservation is:

$$C_p \rho_f \frac{\partial T_f}{\partial t} + \frac{C_p \rho_f \mathbf{V}_f \bullet \nabla T_f}{\phi} = \frac{\partial p_f}{\partial t} + \frac{\mathbf{V}_f \bullet \nabla T_f}{\phi} + \nabla \bullet \left(\kappa_f \nabla T_f \right) + \frac{h_v}{\phi} (T_s - T_f) \qquad (8)$$

h_v in the above equation is called the volumetric heat transfer coefficient. Finally, the heat conduction equation of the porous media is:

$$c_s \rho_s \frac{\partial T_s}{\partial t} = \nabla \bullet \left(\kappa_s \nabla T_s \right) - \frac{h_v}{1-\phi} (T_s - T_f) \qquad (9)$$

2.2 Chemical Model

In this study, 11 species and 7 chemical reactions were considered:

$$O_2, N_2, O, NO, N, NO^+, e^-, N^+, O^+, Ar, Ar^+$$

$$O_2 \rightleftarrows 2\,O \qquad (10)$$

$$N_2 + O_2 \rightleftarrows 2NO \qquad (11)$$

$$N_2 \rightleftarrows 2\,N \qquad (12)$$

$$NO^+ + e^- \rightleftarrows NO \qquad (13)$$

$$N^+ + e^- \rightleftarrows N \qquad (14)$$

$$O^+ + e^- \rightleftarrows O \qquad (15)$$

$$Ar^+ + e^- \rightleftarrows Ar \qquad (16)$$

The chemical equilibrium composition is governed by 11 simultaneous equations.

- 7 equilibrium equations
- 3 mass-balance equations
- 1 charge neutrality equation

2.3 Numerical Scheme

2.3.1 External Flow

For the external flow, we adopted the Harten-Yee's upwind TVD scheme to evaluate the numerical flux of the convective terms and used the 2nd order central difference. To take real gas effect into account, the correction was made for the thermodynamic properties and the transport properties listed below. [2],[3]

- Specific heat ratio
- Specific heat
- Sound speed
- Temperature
- Viscosity
- Thermal conductivity

To calculate the chemical equilibrium composition, we have to solve the 11 simultaneous equations, but the 7 equilibrium equations are nonlinear, so they cannot be solve analytically. Therefore, the iterative method

developed by Prabhu [4] was adopted. The Prabhu's method can save computational time by dividing the density-temperature domain into four regions and identifying the "major species", the species that are found in abundance in each of these regions.

Finally, the Baldwin-Lomax model was adopted as the turbulence model. The transition from laminar to turbulence can occur even at hypersonic speeds and cause an increase in aerodynamic heating, hence it is important to take it into account. Baldwin-Lomax model is in the class of what is called the "eddy viscosity model", where the effects of turbulence in the governing equations are included simply by adding an additional term to the transport properties.

$$\mu = \mu_l + \mu_t \tag{17}$$

$$\kappa = \kappa_l + \kappa_t = \frac{\mu_l c_p}{\mathrm{Pr}_l} + \frac{\mu_t c_p}{\mathrm{Pr}_t} \tag{18}$$

2.3.2 Internal Flow and Porous Media

For the internal flow and the heat conduction of the porous media, the present author used the 2nd order central difference to evaluate the partial derivative, and introduced the relaxation parameter to suppress the numerical instability.

2.4 Computational Grid

In the computational grid for the external flow, there are 75 grid points normal to the surface, and 82 grid points along the surface. In the computational grid for the internal flow and porous media, there are 75 grid points normal to the surface and 35 grid points along the surface. Hence, there are 8,775 grid points in total. Fig. 1 shows the grid system. Red grids are for the external flow. The green and blue grids are for the porous material. Coolant air is transpired only in the region of the blue grids.

2.5 Code Validation

2.5.1 Turbulence model

The present author calculated the flow on the adiabatic wall and checked the velocity profile in the boundary layer. Fig. 2 shows its results. Its agreement with the law of the wall, which was confirmed by the experiment, is quite well.

2.5.2 Real Gas Effects

The temperature behind the shock wave is lower under the condition of chemical equilibrium than in the case where the gas is assumed calorically perfect. This is because the kinetic energy of the flow is shared across the all molecular modes of energy and goes into the zero point energy of the product of the chemical reaction. And the lower the pressure is, the more remarkable this effect is. This is because increasing the pressure tends to inhibit the dissociation and the ionization. The code was checked by calculating the flow around the blunt body. Fig. 3 shows its results. The result agrees very well.

2.5.3 Chemical Composition

Chemical equilibrium composition under the constant density was solved. Fig. 4 shows its results. We can see that the dissociation and the ionization occur as the temperature increases. The present author checked that its result agrees very well quantitatively with Prabhu's results.

3. Computational Results and Discussions

3.1 Without Thermal Protection Systems

First of all, the flow around the blunt body without a thermal protection system was calculated. Table 1 shows the computational conditions. The assumption of the chemical equilibrium is valid under this condition. Fig. 5 shows the temperature distribution of the flow field. And Fig. 6 shows the one under the same condition but in the case where the gas is assumed to be calorically perfect. We can see the difference in the shock stand-off distance and the temperature decrease. Fig. 7 shows the mole fractions on the stagnation streamline. We can see that atomic oxygen and nitric oxide are produced as the flow passes through the shock. Fig. 8 shows the aerodynamic heating on the surface. We can see that diffusive heating is about 20% of the total.

3.2 Film Cooling

In this study, the present author assumed that the coolant air chokes in the converging nozzle and reaches to sonic speed at the exit. And the position of the second injection point is changed as a parameter. Table 2 shows the computational condition. Fig. 9 shows the pressure distribution. We can see that flow field is changed by the injection.

To study the effects of film cooling, the decrease in the aerodynamic heating and the one per unit mass flow was calculated. Fig. 10 shows the former, and Fig. 11 shows the latter. For each, we can see that there is the optimal position for the second injection point.

Finally, the present author calculated the increase of the drag and compared its results with that of the case without thermal protection system. Fig. 12 shows the percentage of the increase of the drag. We can see that not only aerodynamic heating but also the drag can be decreased in the case where the second injection point is set near the stagnation point.

3.3 Transpiration Cooling

The transpiration cooling has the disadvantage of the mass flow near the stagnation point becoming insufficient if the coolant air is transpired at the same constant pressure in all areas. This is because the pressure of the external flow is high near the stagnation point. To avoid this, the present author combined film cooling and transpiration cooling, and assumed part of the coolant air is injected through the slit at the stagnation point and the rest is transpired through the porous media in the limited regions on the surface. Table 3 shows the computational condition. Fig. 13 shows the temperature distribution of the media and the velocity vector plot of the transpiring coolant air. We can see that the temperature of the media is cooled down by the transpiration, and the coolant air is transpired almost normal to the surface. Fig. 14 shows the decrease of the average surface temperature of the media per unit mass flow. The less the mass flow is, the more effective the cooling is.

3.4 Comparison between the Cooling Systems

To compare the effects of the film cooling and the transpiration cooling, the present author

removed the isothermal condition for the analysis of film cooling and recalculated it under the same condition of the transpiration cooling. Fig. 15 shows the surface temperature of the media. The transpiration cooling system can keep the surface temperature low in the wide region of the transpiration. Fig. 16 shows the decrease in the average surface temperature of the media. We can see that the transpiration cooling is more effective than the transpiration cooling under the condition of this study.

4. Conclusion

Numerical analysis of the chemical equilibrium flow was conducted. The temperature behind the shock is decreased by real gas effect, and atomic oxygen and nitric oxide are in the majority of the chemical composition under the condition of this study.

In the analysis of film cooling, there is an optimal position for the second injection point. And not only aerodynamic heating but also the drag can be decreased when the second injection point is set near the stagnation point.

Regarding the transpiration cooling, the less the mass flow is, the greater the decrease of the average surface temperature per unit mass flow is.

Finally, two cooling systems were compared. The transpiration can cool down the surface temperature in a wide region and is more effective than film cooling under the condition of this study.

References

[1] Ishii I, Kubota H. Two-Dimensional Material Response of a Transpiration-Cooled System in a Radiative/Convective Environment, *AIAA Journal*, Vol.22, No. 6, pp 831-836, 1984

[2] Srinivasan S, Tannehill J.C. Simplified Curve Fits for the Thermodynamic Properties of Equilibrium Air, NASA RP 1181, 1987

[3] Gupta R.N, Lee K, Thompson R.A, Yos J.M. Calculation and Curve Fits of Thermodynamic and Transport Properties for Equilibrium Air to 30 000 K, NASA RP 1260, 1991

[4] Prabhu R.K, Erickson W.D. A Rapid Method for the Computation of Equilibrium Chemical Composition of Air to 15 000 K, NASA TP 2792, 1988

Table. 1: Computational condition for the case of no thermal protection system

Altitude [km]	40
Velocity [m/sec]	2696.3
Mach Number	8.5
Isothermal Wall Temperature [K]	2000

Table. 2: Computational condition for film cooling

Injection Temperature [K]	280
Injection Pressure [MPa]	0.025, 0.030, 0.035
Isothermal Wall Temperature [K]	2000

Table. 3: Computational condition for transpiration cooling

Injection Temperature [K]	260
Injection Pressure [MPa]	0.025, 0.030, 0.035
Porosity	0.4, 0.6, 0.8

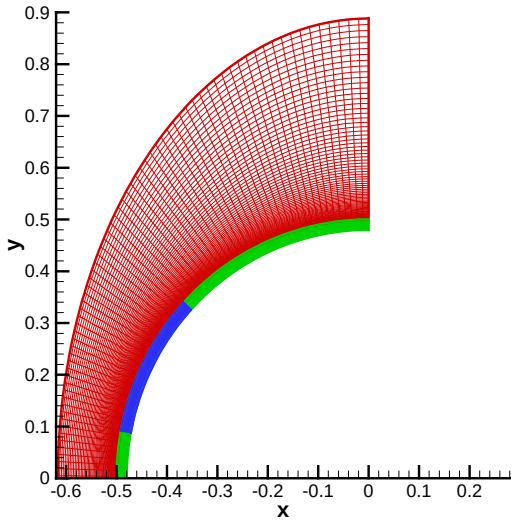

Fig. 1: Computational grid

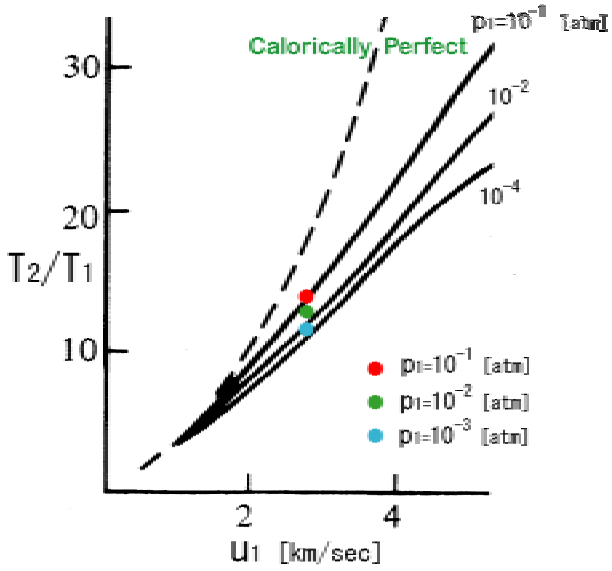

Fig. 3: Temperature behind the shock

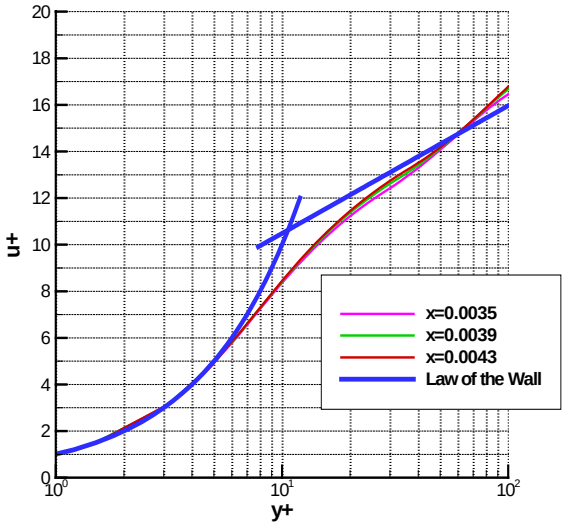

Fig. 2: Velocity profile in the boundary layer

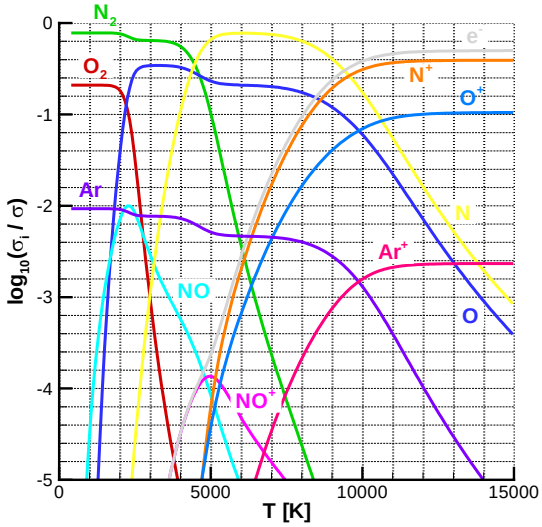

Fig.4: Chemical composition of air

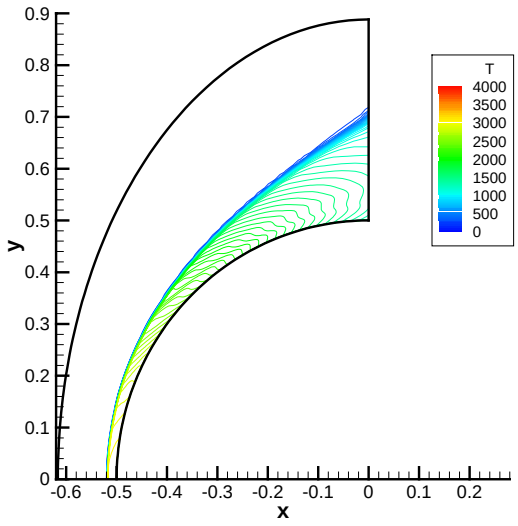

Fig. 5: Temperature distribution: chemical equilibrium

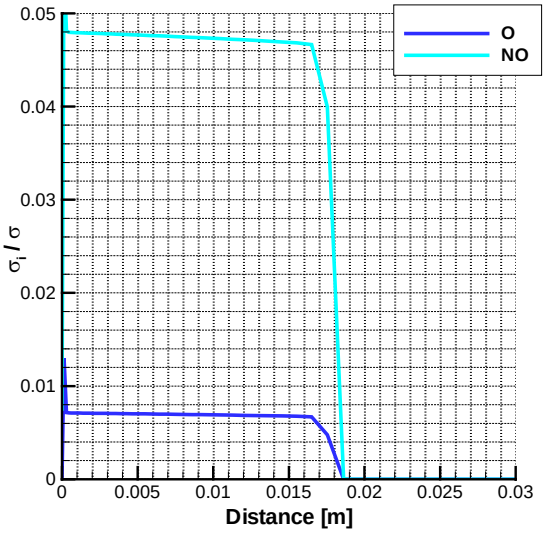

Fig. 7: Mole fraction on the stagnation streamline

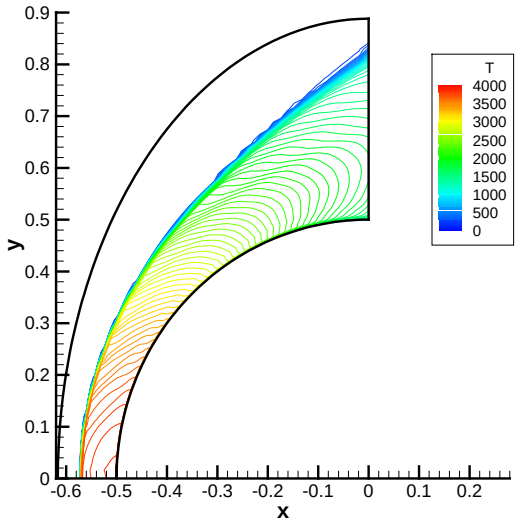

Fig. 6: Temperature distribution: calorically perfect

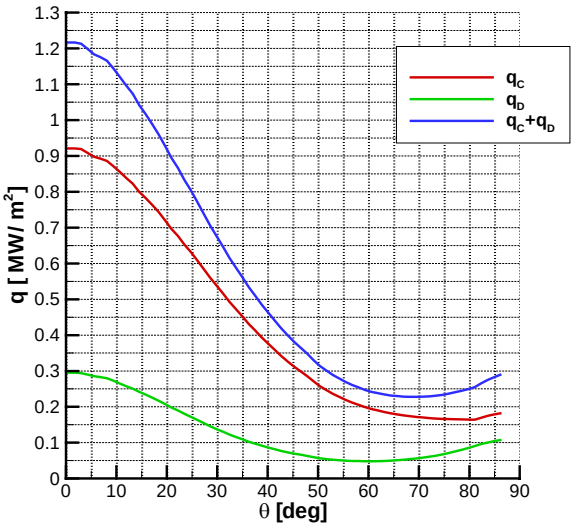

Fig. 8: Aerodynamic heating on the surface

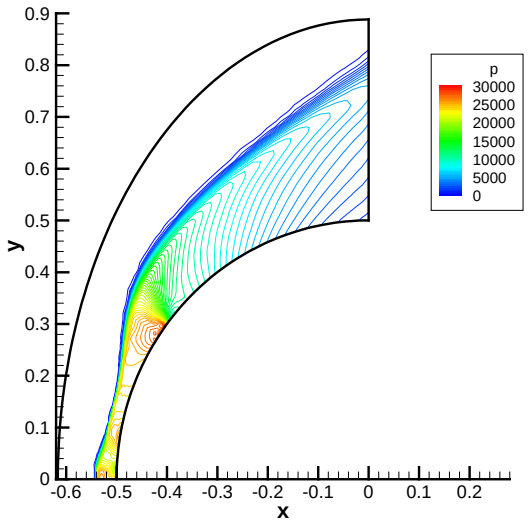

Fig. 9: Pressure distribution

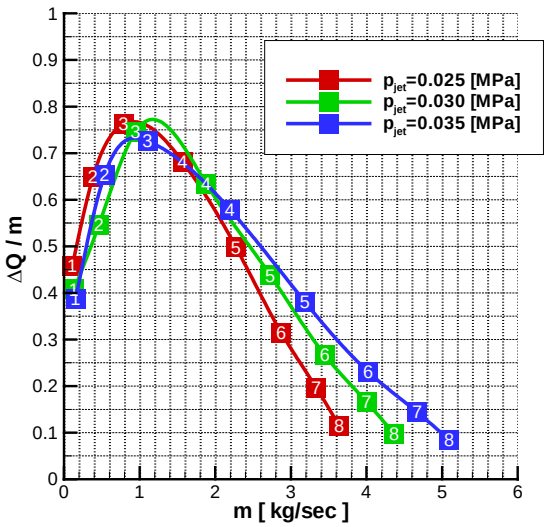

Fig. 11: Decrease in aerodynamic heating per unit mass flow

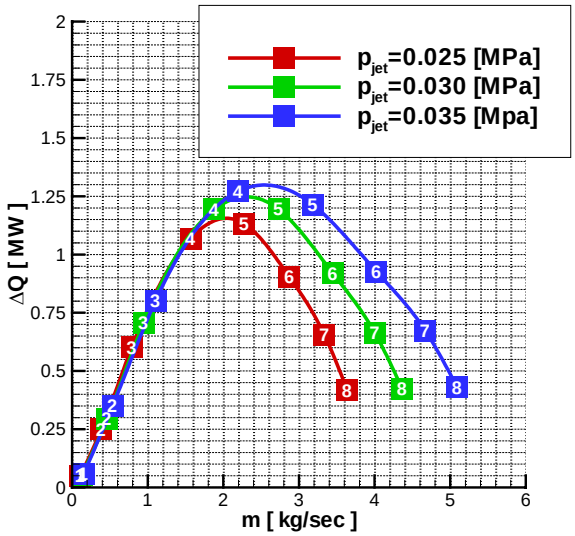

Fig. 10: Decrease in aerodynamic heating

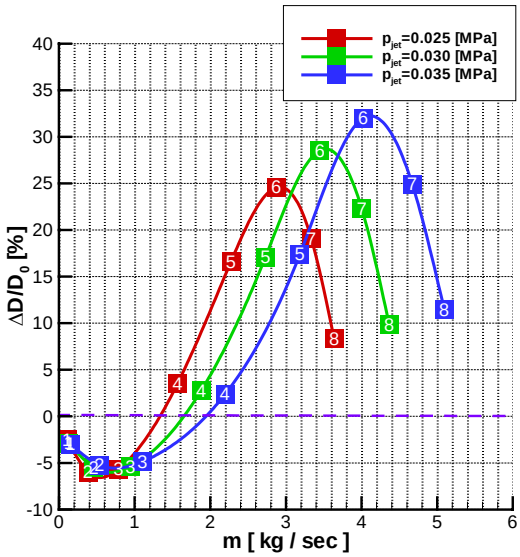

Fig. 12: Increase of drag

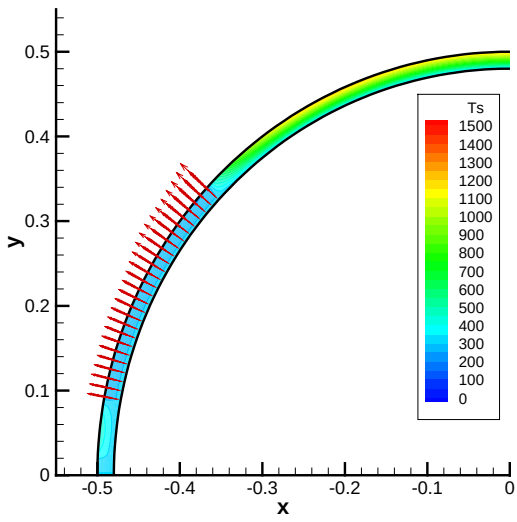

Fig.13: Temperature distribution: transpiration cooling

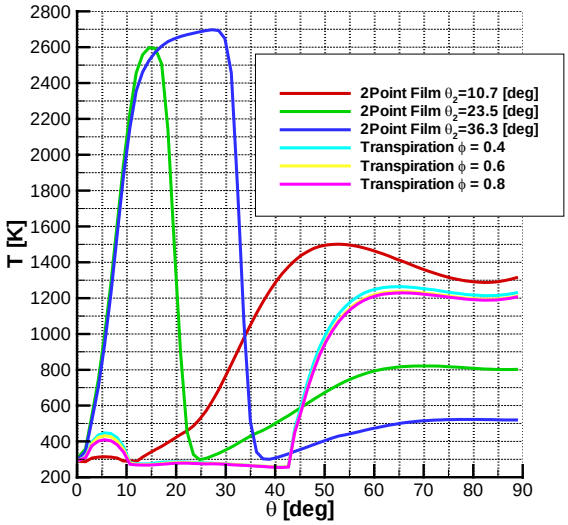

Fig.15: Surface temperature of the media

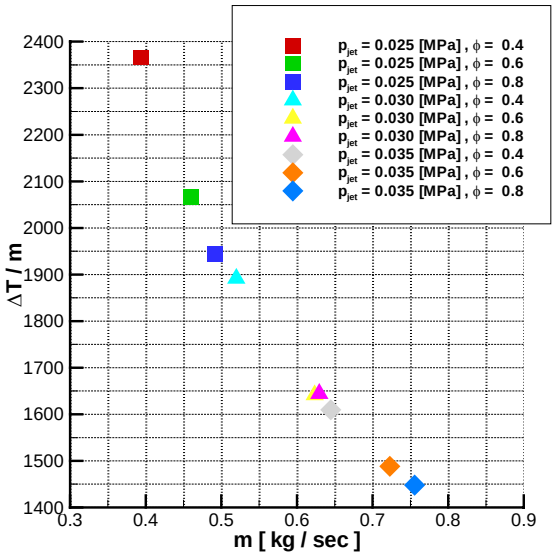

Fig. 14: Decrease in average surface temperature of the media per unit mass flow

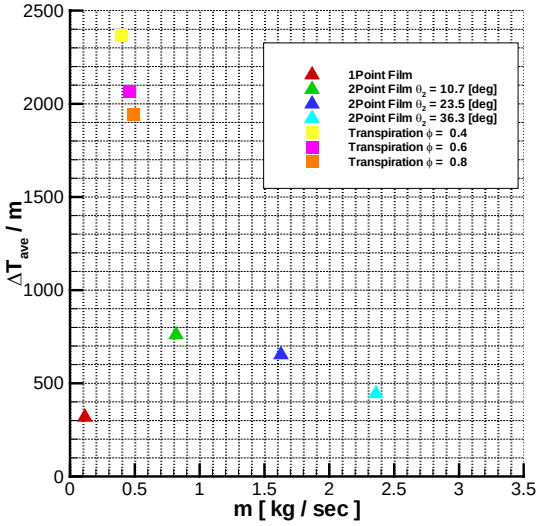

Fig. 16: Decrease in average surface temperature of the media per unit mass flow